ELSEVIER

Contents lists available at ScienceDirect

Acta Materialia

journal homepage: www.elsevier.com/locate/actamat



Full length article

Explosive martensitic transformation of supercooled austenite in CuZr-based thin-film shape memory alloys



Yucong Miao, Joost J. Vlassak*

John A. Paulson School of Engineering and Applied Sciences, Harvard University, Cambridge, MA 02138, United States

ARTICLE INFO

Article history: Received 2 July 2020 Revised 30 August 2020 Accepted 30 August 2020 Available online 4 September 2020

Keywords: Shape memory alloy Martensitic transformation Nanocalorimetry Supercooling

ABSTRACT

CuZr-based alloys are being considered as potential shape memory alloys for use in high-temperature applications. We have conducted a study on the effects of several alloying elements on the shape memory properties of these alloys using polycrystalline thin-film samples. Here we report on the explosive formation of martensite in supercooled CuZr, CuZrNi and CuZrCo samples. This explosive transformation behavior is characterized by the following observations: 1) The high-temperature austenitic phase can be supercooled below the martensite finish temperature M_f . At a critical temperature below M_f , austenite transforms to martensite across the entire sample in less than a microsecond. 2) The critical temperature has a narrow distribution and decreases slightly with higher cooling rate. 3) Observation of supercooling and explosive transformation behavior depends on the temperature history above the austenite finish temperature A_f . If a sample is quenched immediately after heating above A_f , martensite forms gradually on cooling below M_s ; if a sample is allowed to dwell a few seconds above A_f , the martensite forms explosively. We suggest that the gradual transformation proceeds by martensite growth on defects that accumulate during successive transformation cycles. If the sample is allowed to dwell at a temperature above A_{f_t} however, these defects are annihilated and the transformation is nucleation-limited. Nucleation of martensite then requires significant supercooling. The defect annihilation process is highly sensitive to temperature and has an apparent activation energy of 326 kJ/mol, which is too large for a simple diffusion-limited process. Transmission electron microscopy of CuZrCo samples suggests that the defects may be related to the presence of residual martensite.

© 2020 Acta Materialia Inc. Published by Elsevier Ltd. All rights reserved.

1. Introduction

Shape memory alloys (SMAs) rely on a thermoelastic transformation between a high-symmetry austenitic and a low-symmetry martensitic phase for their special properties. The large recoverable strain and energy density associated with the transformation make SMAs widely useful in engineering applications, such as actuators and dampers [1–3]. CuZr-based SMAs have higher martensite transformation temperatures than commercially available SMAs based on NiTi, and are being evaluated for use in high-temperature applications [4–6]. The addition of Ni to CuZr increases the transformation temperature [4,7] and has the potential to reduce the hysteresis [7], which can be quite large in some CuZr-based SMAs [4,8].

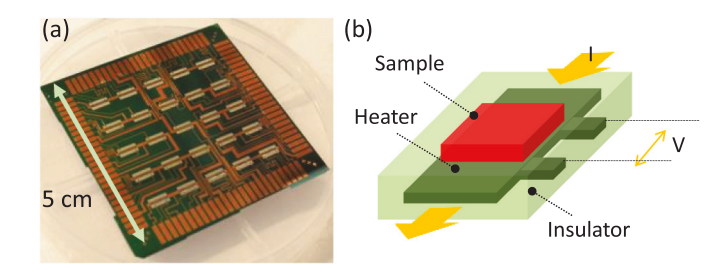
In most shape memory alloys, the martensite that is responsible for the shape memory properties forms gradually on cooling below the martensite start temperature M_S and it is fully formed

* Corresponding author.

E-mail address: vlassak@seas.harvard.edu (J.J. Vlassak).

when the temperature reaches the finish temperature M_f [9]. The martensitic transformation (MT) is athermal, i.e., no thermal activation needed. There are, however, a number of examples where martensite forms differently. Machlin and Cohen first reported both explosive and isothermal martensite formation in non-shape memory Fe-Ni alloys [10,11]. A succession of small bursts is also observed during the formation of martensite in Cu-Al-based shape memory alloys, as a result of jerky propagation of the interface between the austenite and martensite [12,13].

In this paper, we report on explosive transformation behavior observed using nanocalorimetry in CuZr, CuZrNi and CuZrCo thinfilm samples supercooled below M_f . We attribute this behavior to the fact that the formation of martensite in these samples is nucleation-limited. The transformation behavior is unusual in that it depends sensitively on the thermal history of the samples. If the austenite is quenched immediately after heating above A_f , martensite forms gradually on cooling below the martensite start temperature M_S as it does in most alloy systems. If, however, the austenite is allowed to dwell for a few seconds above A_f , the marten-



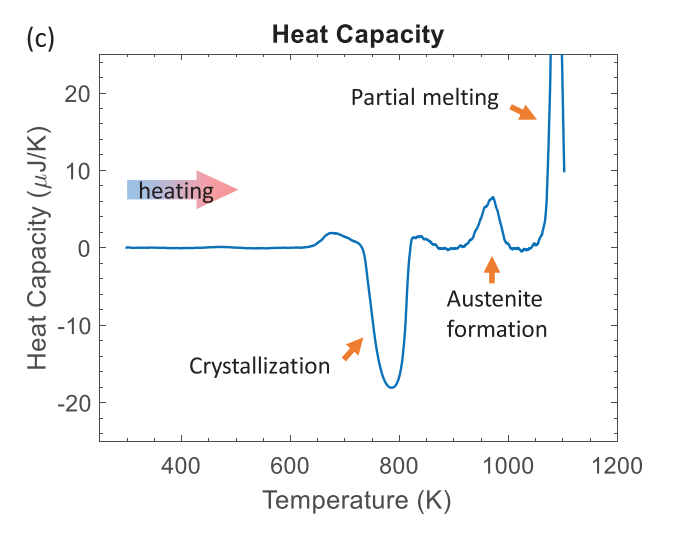


Fig. 1. (a) Picture of a sensor array with 25 nanocalorimetry sensors. (b) Schematic of a single sensor. (c) Phase transformations during the heat treatment of an as-deposited, amorphous $Cu_{40}Zr_{50}Ni_{10}$ sample.

site forms explosively, resulting in a complete transformation of the samples to martensite in less than a microsecond.

2. Experimental

2.1. Nanocalorimetry system

All heat treatments and measurements were performed on thin-film samples using a nanocalorimetry setup [6,14]. The setup relies on a custom-built sensor and data acquisition system. Fig. 1a and 1b show a sensor array and a schematic of a single sensor, respectively. The sensors are fabricated using silicon microfabrication techniques, the details of which can be found in our previous work [14]. Each sensor consists of a tungsten heating element/thermistor embedded within a freestanding silicon nitride membrane. The membrane protects the heating element from oxidation and provides support, while limiting conductive heat loss to the surroundings. The heating rate ranges from zero for isothermal measurements to 10^6 K/s [15]. Measurements are performed in a high-vacuum chamber to prevent oxidation of the sample and heat loss to the ambient air.

In a typical measurement, a current profile is applied to the tungsten thermistor. The resistance of the tungsten is obtained by measuring the voltage drop across the sample region (Fig. 1b). This resistance is then mapped to temperature using the temperature coefficient of resistance λ of the tungsten thermistor,

$$R = R_0(1 + \lambda(T - T_0)), \tag{1}$$

where R is the resistance of the thermistor at temperature T, and R_0 the resistance at the ambient temperature T_0 . On heating, the energy balance for the sensor dictates that

$$P = V \cdot I = C_p \cdot \beta + L. \tag{2}$$

In this expression, P is the power supplied to the sensor, V is the potential drop across the heating thermistor, I is the current through the thermistor, C_p is the heat capacity of the sample and sensor addendum, β is the heating rate, and L is heat loss to the environment through radiation and conduction. The contribution of the heat loss in Eq. (2) can be largely eliminated by making differential measurements using an empty sensor as a reference [6]. In that case, the differential heat capacity is

$$\Delta C_p = C_p^{\text{sam}} - C_p^{\text{ref}} \approx I \cdot \left(\frac{V_{\text{sam}}}{\beta_{\text{sam}}} - \frac{V_{\text{ref}}}{\beta_{\text{ref}}} \right), \tag{3}$$

where the subscripts refer to measurements for the sensor with the sample and the empty reference sensor, respectively. To reduce noise, $\beta_{\rm ref}$ can be averaged over a number of measurements that use an identical current profile; $\beta_{\rm sam}$ can be derived from $\beta_{\rm ref}$ and the differential voltage ΔV using

$$\beta_{\text{sam}} = \beta_{\text{ref}} \frac{R_0^{\text{ref}}}{R_0^{\text{sam}}} + \frac{1}{I\lambda R_0^{\text{sam}}} \frac{d\Delta V}{dt} - \frac{\Delta V}{I^2 \lambda R_0^{\text{sam}}} \frac{dI}{dt}.$$
 (4)

Additional small corrections for heat loss and the temperature-dependence of the heat capacities of the sensors are discussed in detail in reference [6]. Using a Sn sample with 3 nm thickness and a heating rate of 40,000 K/s, we have demonstrated that the root-mean-square noise of ΔC_p can be as small as 6 nJ/K at 400 K [6].

2.2. Sample preparation and characterization

Thin-film samples of CuZr, CuZrNi and CuZrCo were prepared directly on top of the calorimetry sensors by magnetron cosputtering from single elemental targets (acquired from Kurt J. Lesker Co.; purity: Zr > 99.2%, Cu > 99.999%, Ni > 99.995%, Co > 99.95%; 50.8 mm diameter) in a high-vacuum chamber (AJA ATC-1800). To prevent reaction between the sample and the underlying silicon nitride, a layer of 20 nm HfO2 was grown on top of the sensors by means of atomic layer deposition (ALD) prior to sample deposition (Cambridge NanoTech ALD System). The base pressure of the vacuum chamber was better than 5×10^{-7} Torr and the Ar working gas pressure during deposition was 5 mTorr. The power of the Zr target was fixed at 160 W, while the power supplied to the other targets was varied to produce samples with compositions of $Cu_{51}Zr_{49}$, $Cu_{47}Zr_{49}Co_4$, and $Cu_{50-x}Zr_{50}Ni_x$. The compositions were confirmed using X-ray photoelectron spectroscopy (Thermo Scientific K-Alpha Plus XPS System) with Ar ion depth profiling. The thicknesses of the samples were in the 400-500 nm range and were controlled by deposition time. A shadow mask was used to limit deposition to the sample areas of the sensors (Fig. 1b).

All as-deposited samples were amorphous, and were heattreated using the nanocalorimetry sensors to obtain the austenitic phase. The phase evolution of a Cu₄₀Zr₅₀Ni₁₀ sample during heat treatment is shown in Fig. 1c. The sample crystallized at approximately 780 K, resulting in a strong exothermic signal in the heat capacity curve [7,16]. The small feature immediately prior to crystallization is the glass transition [17]. The austenitic phase is formed in a eutectoid reaction between the crystallization products at approximately 970 K. If a sample is heated through the eutectoid peak only, it does not transform to martensite on cooling. We attribute this to insufficient ordering of the austenitic phase [6]. Planes et al. have reported an order-disorder transformation in the high-temperature phases in some Cu-based shape memory alloys [18]. To obtain an austenitic phase that transforms to martensite on cooling, a lengthy heat treatment above the eutectoid temperature or a partial melting treatment needs to be performed on these samples. The partial melting treatment resulted in austenite with 100 to 300 nm grains. Transmission electron microscopy characterization was performed using a JEOL ARM-200F TEM. Crosssectional TEM samples were prepared from the samples on the

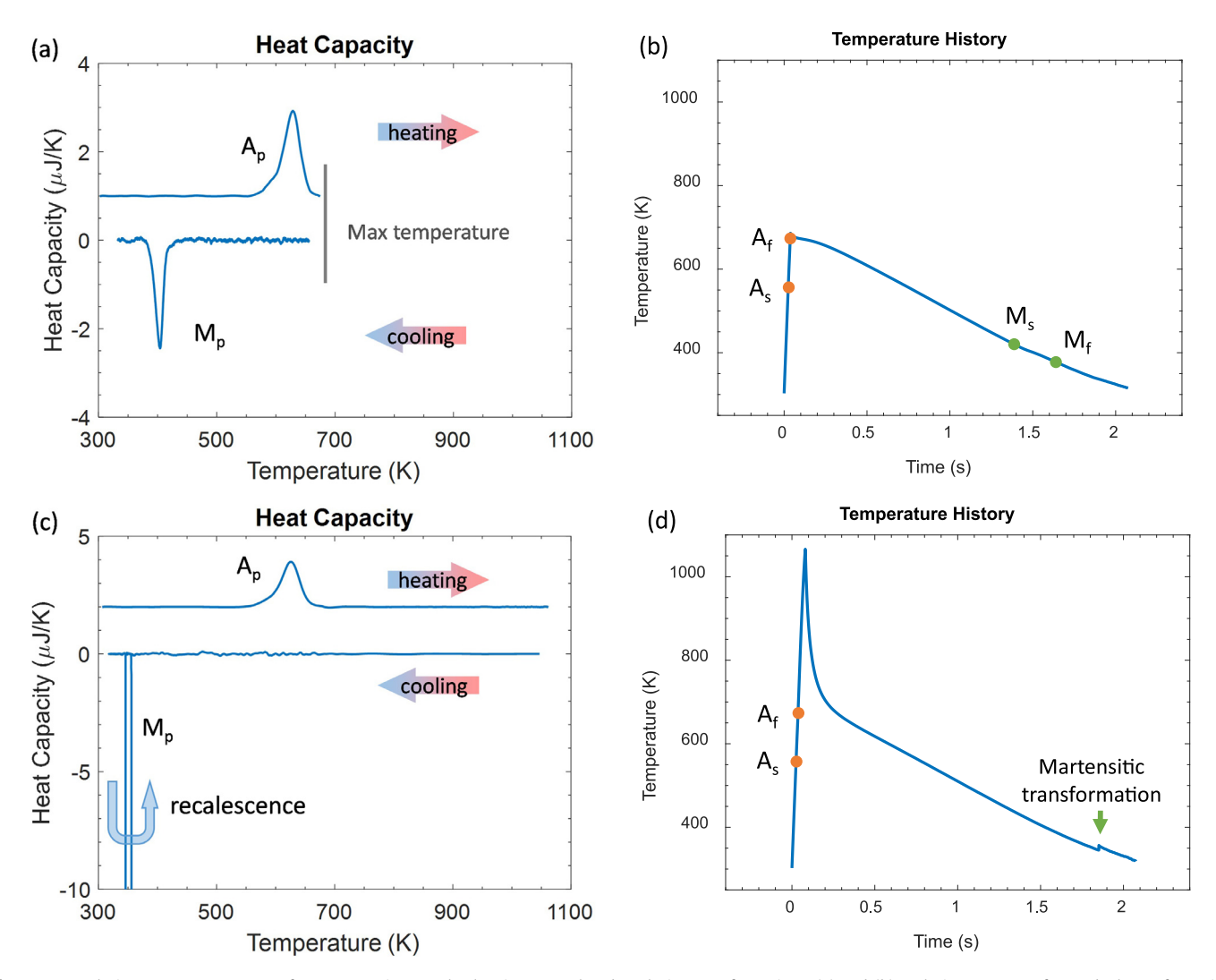


Fig. 2. Nanocalorimetry measurements of a $Cu_{40}Zr_{50}Ni_{10}$ sample showing normal and explosive transformations. (a) and (b): Calorimetry scan of a gradual transformation and corresponding thermal history. (c) and (d): Calorimetry scan of an explosive transformation and corresponding thermal history. Heating and cooling curves in the calorimetry scans have been offset for clarity.

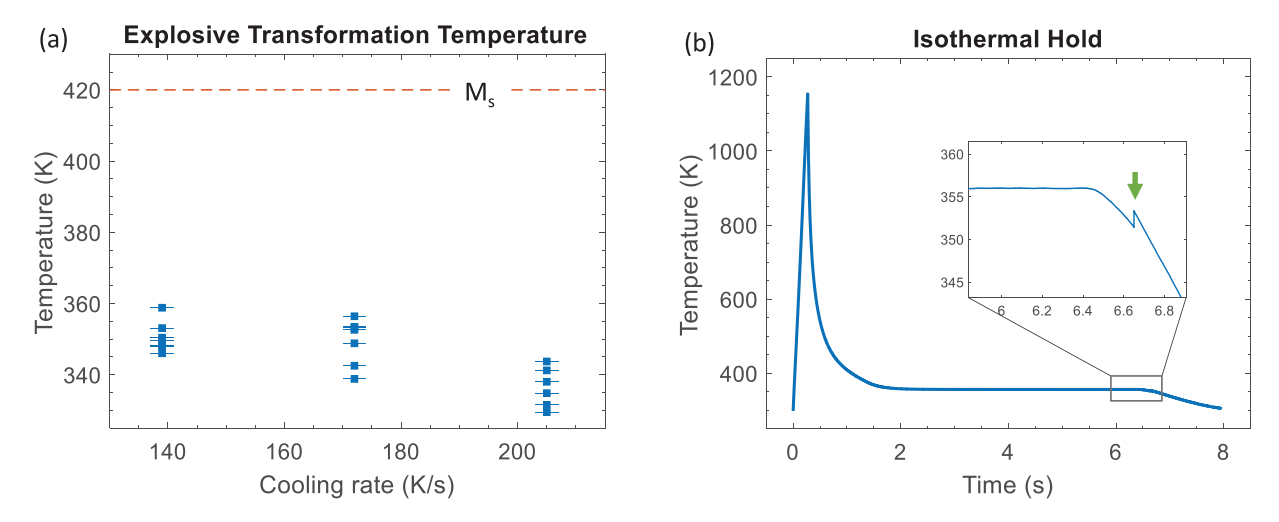
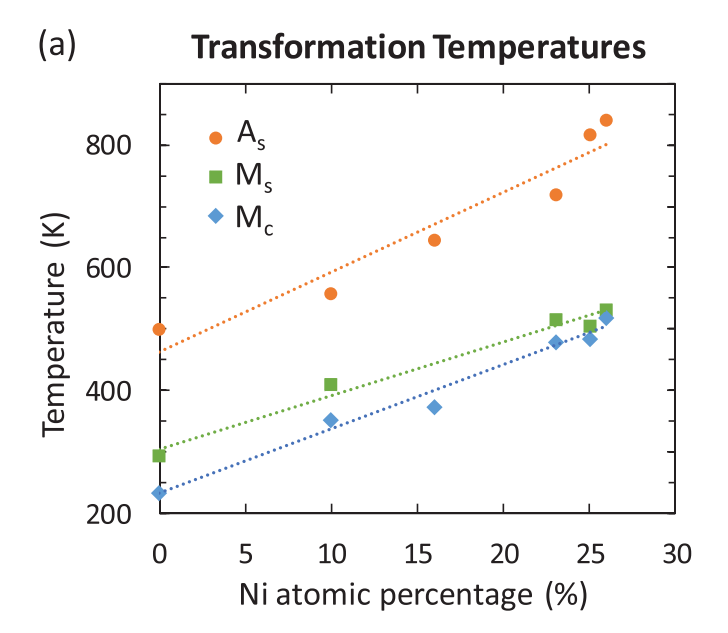


Fig. 3. (a) Critical transformation temperatures M_c as a function of cooling rate measured on a $Cu_{40}Zr_{50}Ni_{10}$ sample. (b) Temperature history for a $Cu_{40}Zr_{50}Ni_{10}$ sample with an isothermal treatment at 5 K above the critical temperature. The explosive transformation is marked by the arrow.



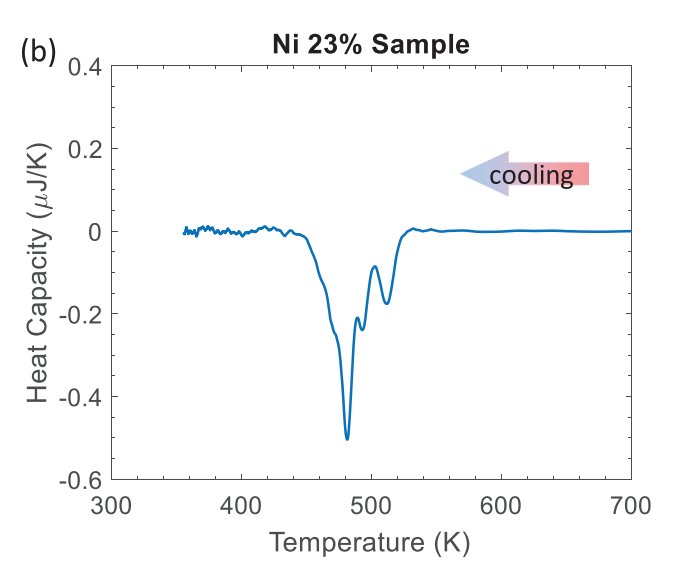


Fig. 4. (a) Transformation temperatures for different compositions of CuZrNi. The Zr content is fixed at $50\pm2\%$ while Ni and Cu are allowed to change. $A_{\rm S}$ is the austenite starting point, $M_{\rm S}$ is the gradual MT starting point, and $M_{\rm C}$ is the critical temperature for explosive transformation. The results have an estimated error of ±5 K. The trend lines serve as guides to the eye. When the Ni content is above 25%, the supercooling effect is no longer observed. (b) Transformation trace of a CuZrNi sample with 23 at.% Ni shows a series of bursts.

nanocalorimetry sensors using a focused ion beam lift-out technique (Helios 660 Dual-Beam FIB).

3. Results

3.1. Characteristics of the supercooled martensitic transformation

To investigate the formation of the martensitic phase, heat-treated samples were subjected to various nanocalorimetry cycles at a nominal heating rate of 10,000 K/s. The results of these experiments are summarized in Figs. 2–7. Fig. 2 shows the calorimetry results for two different thermal cycles on the same sample of $\text{Cu}_{40}\text{Zr}_{50}\text{Ni}_{10}$, along with the corresponding temperature histories. The main difference between the two thermal cycles is the maximum temperature reached during the cycles. In both cases, the sample has a clear martensite-to-austenite transformation on

heating and an austenite-to-martensite transformation on cooling. It is evident, however, that the maximum temperature that the sample is exposed to has a significant effect on how the martensite forms on cooling. In Fig. 2a, the sample is cooled immediately after reaching A_f . The result is a gradual transformation between 420 K and 380 K, i.e., behavior similar to what is observed in most shape memory alloys. In Fig. 2c, the sample is heated to a temperature that is approximately 400 K higher than A_f . The transformation to martensite now occurs abruptly at 345 K and the entire sample transforms nearly instantaneously, causing a sudden spike in temperature. This explosive transformation occurs at a temperature well below the M_f observed in the low-temperature thermal cycle.

Remarkably, in the explosive transformation, the austenite transforms to martensite throughout the entire sample in less than one microsecond - the transformation occurs between two consecutive data points obtained at an acquisition rate of 10⁶ Hz. Assuming the transformation starts in just one location of the sample, it is possible to obtain a lower bound on the propagation speed of the transformation. The thin-film sample has lateral dimensions of 3.6 mm \times 0.8 mm. If the transformation starts in the center of the sample, the propagation speed is at least 1800 m/s, a significant fraction of the speed of sound in these materials. A comparison of the enthalpies of transformation on heating and cooling confirms that the entire sample transforms to martensite in a single burst. Given that there exists some temperature non-uniformity in the samples during the measurement, these observations suggest that the formation of martensite is triggered by a single nucleation event and that the transformation then propagates across the entire sample, probably as a result of a stress wave, rather than by individual grains transforming independently on reaching a critical temperature – i.e., the transformation is autocatalytic.

To examine the kinetics of the nucleation event, twenty calorimetry measurements were performed at three different cooling rates on the same $Cu_{40}Zr_{50}Ni_{10}$ sample, after heating to the same maximum temperature of 1060 K. Fig. 3a summarizes the results. It is evident that there is significant scatter in the critical temperature for a fixed cooling rate and that the critical temperature decreases slightly with increasing cooling rate. Fig. 3b shows that if the sample is held for five seconds at a temperature slightly above the critical temperature but below M_f , no transformation is observed for the duration of the isothermal hold. On subsequent cooling, the sample transforms explosively. Evidently, nucleation of the martensitic phase in the explosive transformation is a stochastic event with only a slight temperature dependence.

3.2. Effect of composition on transformation behavior

Further experiments show that explosive transformations may be observed in CuZr, CuZrNi, and CuZrCo alloys over a range of compositions. Fig. 4a shows how the various transformation temperatures $(M_s, M_c, \text{ and } A_s)$ change with Ni content in $ZrCu_{1-x}Ni_x$ alloys. All three temperatures increase with increasing Ni content, but M_c increases more rapidly than M_s . As a result, the degree of supercooling decreases as the Ni content increases and supercooling disappears at approximately 25 at.% Ni. As illustrated in Fig. 4b, the transformation is then completed in a series of small bursts alongside a gradual transformation. Nucleation of martensite is clearly much easier at this composition. Because the temperature is above M_f , nucleation at one site does not trigger transformation of the entire sample. Fig. 5 shows calorimetric curves for the Cu₅₁Zr₄₉ and Cu₄₇Zr₄₉Co₄ alloys. Both samples exhibit supercooling behavior, but the degree of supercooling varies. The supercooling is approximately 60~K for the $Cu_{51}Zr_{49}$ sample, slightly less than for $Cu_{40}Zr_{50}Ni_{10}$, while the supercooling for the $Cu_{47}Zr_{49}Co_4$ sample is only about 15 K. The difference suggests that supercool-

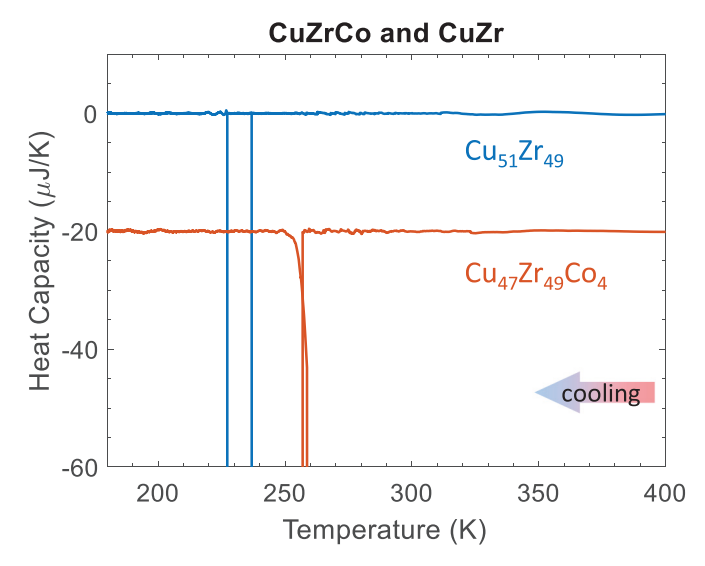


Fig. 5. Explosive transformations in $Cu_{47}Zr_{49}Co_4$ and CuZr. CuZr shows more supercooling and more recalescence than $Cu_{47}Zr_{49}Co_4$. The results have been offset for clarity.

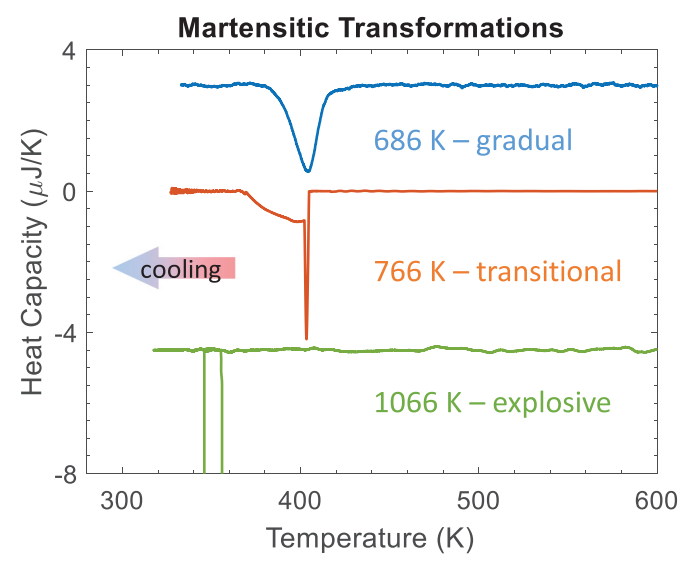


Fig. 6. Transformations for a $Cu_{40}Zr_{50}Ni_{10}$ sample heated to different maximum temperatures. The low-temperature scan (top) shows a gradual transformation; the high-temperature scan (bottom) shows an explosive transformation; the intermediate-temperature scan (middle) shows transitional behavior.

ing behavior can be drastically altered by alloying, even though electron microscopy shows that there is little or no change in the microstructure.

3.3. Effect of temperature history on the martensitic transformation

Fig. 6 demonstrates that the explosive character of the martensitic transformation depends sensitively on the thermal history above A_f . In the figure, we compare cooling curves for the same $\mathrm{Cu}_{40}\mathrm{Zr}_{50}\mathrm{Ni}_{10}$ sample that was thermally cycled to three different temperatures. Before each measurement in the figure, three high-temperature cycles were performed on the sample to ensure that the starting conditions for each measurement were exactly the same. In the low-temperature cycle, the sample was quenched immediately upon reaching $A_f=680$ K. This treatment results in a gradual transformation of austenite to martensite on cooling, allowing determination of the M_S and M_f temperatures. The high-temperature cycle results in an explosive transformation, while the

cycle to an intermediate temperature yields a transitional case – there is no significant undercooling, and transformation behavior is partly explosive, partly gradual.

The maximum temperature to which the sample is cycled also has an impact on the stability of the transformation. Fig. 7 compares the martensite-to-austenite transformation peak for $\text{Cu}_{40}\text{Zr}_{50}\text{Ni}_{10}$ samples that have been cycled to different temperatures. In the low-temperature cycles, the peak gradually degrades – the height of the peak decreases, the position of the peak shifts to higher temperatures, and the peak becomes broader. From the first scan to the last, the enthalpy release decreases by 47%, indicating that the amount of material participating in the transformation decreases with cycling. In the high-temperature cycles, by contrast, the martensite transformation peak is stable with no changes in either peak position or height.

3.4. Kinetics of defect annihilation

Our results suggest the following picture of the martensitic transformation in these samples: Initial nucleation of the martensitic phase in pristine austenite is difficult. As a result, the samples can be supercooled significantly below the M_f temperature and they transform explosively once the first martensite nucleus forms. This process is autocatalytic and aided by a stress wave that propagates through the entire sample. However, if the samples are thermally cycled through the reverse transformation, defects are generated that make it easier for the martensite to nucleate and the transformation occurs gradually. As the number of cycles increases, defects accumulate and less material participates in the transformation. If the samples are exposed to a temperature that is significantly higher than A_f , the defects disappear and the transformation becomes explosive once more.

To examine the nature of the defects that serve as easy nucleation sites for the gradual transformation, a set of annealing experiments was designed to explore the kinetics of the defect annihilation process. All experiments were performed on a Cu₄₀Zr₅₀Ni₁₀ sample with $A_f = 680$ K. Prior to each anneal, the sample was cycled two times to 1020 K (to annihilate defects) and two times to 700 K (to generate defects), ensuring that the sample had a same amount of defects before the anneal. The sample was then heated to a temperature between 735 K and 780 K, annealed isothermally for a period of time, and finally cooled through the martensitic transformation. We interpret the observations in these experiments as follows: During the isothermal anneal, defects are cleared from a fraction of the sample volume. On cooling, the transformation to martensite is then explosive, gradual, or transitional depending on how many defects are annihilated during the anneal. Table 1 lists the fraction of martensite formed in the explosive transformation as a function of annealing conditions. This fraction was calculated from the sudden temperature jump in the sample and may be used as a measure of the defect annihilation rate r when divided by the anneal time. Notice that only experiments that result in less than 100% annihilation can be used towards the analysis. Fig. 8 shows an Arrhenius graph of the annihilation rate r. If the annihilation process is thermally activated, the slope of the graph yields the activation energy of the annihilation process. The value obtained from Fig. 8 is 326 kJ/mol ($\pm 12\%$). This value is very high, and a factor two or three higher than the activation energy for diffusion in these alloys (96 to 136 kJ/mol) [19,20]. Thus, this experiment seems to rule out defects that may be annihilated by diffusion alone and suggests a more complicated process.

Transmission electron microscopy was performed on two $Cu_{47}Zr_{49}Co_4$ samples to find microscopic evidence for defects that could serve as easy nucleation sites. This particular alloy was selected because its M_s temperature (272 K) is below room temperature, making it possible to observe the austenite phase in

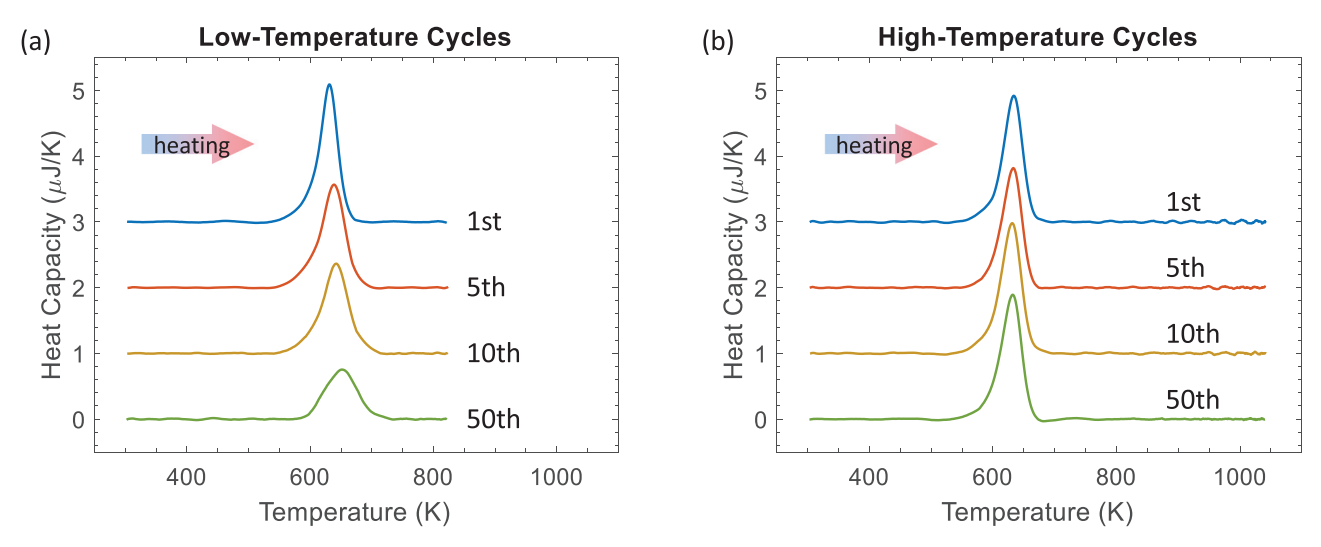


Fig. 7. Calorimetry scans of the austenite transformation as a function of the number of thermal cycles for $Cu_{40}Zr_{50}Ni_{10}$. (a) If the maximum temperature is 830 K, the transformation peak shifts and decreases with the number of cycles; (b) if the maximum temperature is 1045 K, the transformation peak is stable.

Table 1 Results of $Cu_{40}Zr_{50}Ni_{10}$ anneal experiments. The fraction of martensite formed in the explosive transformation is determined from the temperature rise induced by the explosive transformation divided by the temperature rise induced by a complete explosive transformation. The table only lists anneal sessions with less than 100% completion.

Anneal temperature (K)	Anneal time (s)	Fraction of explosive MT resulting from anneal (fraction of unity)
735	1	0.310
735	2	0.388
735	7	0.415
737	0.5	0.075
745	1	0.275
750	1	0.788
755	0.5	0.358
755	1	0.850
764	0.3	0.262
777	0.3	0.715
780	0.1	0.365

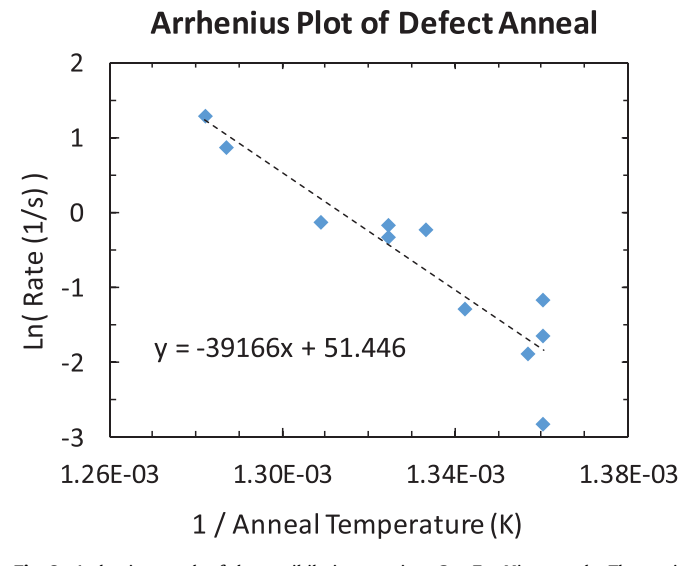


Fig. 8. Arrhenius graph of the annihilation rate in a $Cu_{40}Zr_{50}Ni_{10}$ sample. The annihilation rate is defined as the fraction of martensite that forms explosively divided by the corresponding anneal time.

the microscope without the temperature dropping below M_s . The two samples were subjected to different treatments as illustrated in Fig. 9. The low-temperature cycled (LT) sample should have defects accumulated from the nanocalorimetry cycles, while the

high-temperature cycled (HT) sample should not. Typical TEM micrographs of the two samples are shown in Fig. 10. It is evident from the micrograph in Fig. 10, and others, that the LT sample has martensite plates in multiple grains even though it was cooled from a temperature greater than A_f to a temperature above M_s . The diffraction pattern in Fig. 10b shows the Cm space group with (021) twin planes, which is consistent with previous reports [7,21,22]. The HT sample, on the other hand, is fully austenitic. Densely packed stacking faults in the form of dark stripes are present in both samples. The micrographs combined with the isothermal annealing experiments suggest that it takes some time for martensite to fully transform to austenite, even at temperatures greater than A_f . The residual martensite, in turn, makes it easier for the austenite to transform to martensite on cooling because no nucleation is required.

4. Discussion

In many alloys, the martensitic transformation is athermal – martensite forms when the austenitic phase is cooled below M_s and the volume fraction of martensite is a function of temperature, not time. There are, however, a number of observations in the literature where martensite forms in bursts [10–12]. Examples that have been studied in some detail include Fe-Ni alloys, where the austenitic phase is a solid solution with very few martensite nucleation sites [10,11,23]. Machlin and Cohen have reported that up to 25% of the martensite may be formed explosively at a temperature below M_s [10], after which the martensitic transformation proceeds

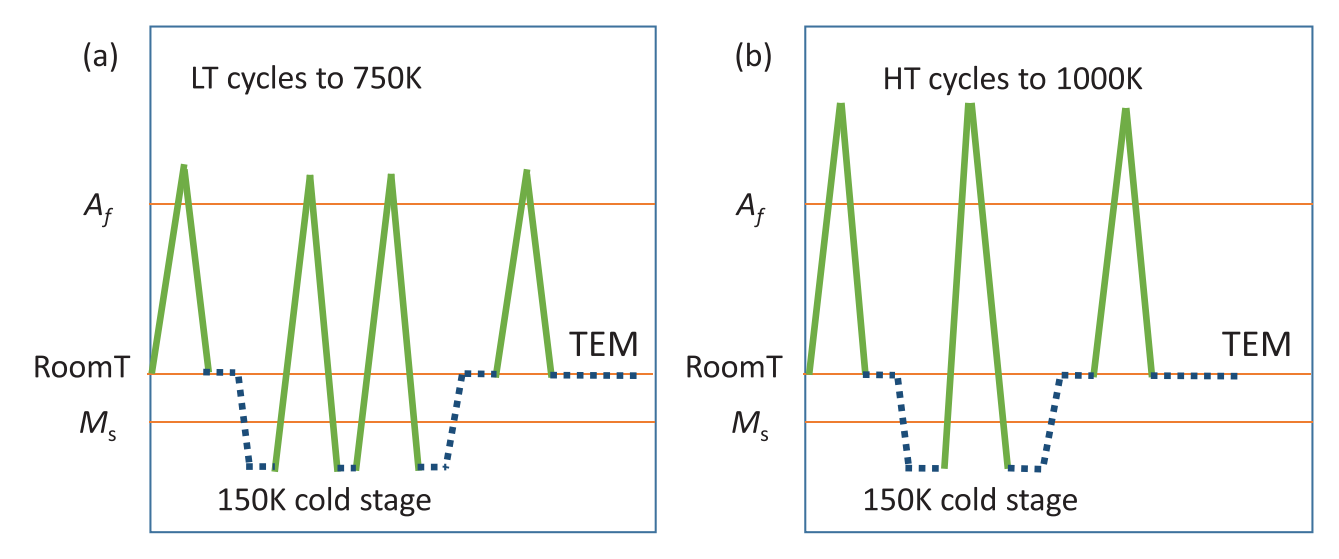


Fig. 9. Heat treatment history of (a) low-temperature cycled and (b) high-temperature cycled $Cu_{47}Zr_{49}Co_4$ samples. The thick solid lines represent calorimetry cycles. The dashed lines represent sample transfers. The thin lines mark A_f , room temperature, and M_s .

isothermally until it reaches a characteristic volume fraction that is a function of temperature. Turnbull and Cohen have suggested that martensite in Fe-Ni nucleates on heterogeneous sites [11,24]. Samples with fewer heterogeneous sites are then more likely to be supercooled below M_s . A succession of small bursts has also been observed during the formation of martensite in CuZnAl alloys, as a result of jerky propagation of the M-A interface. Planes et al. have associated this behavior with the β -2H martensitic transformation [12,13]. When the composition changes in these alloys, the type of martensite changes from 2H to 18R and the transformation becomes smooth. This transition to 18R martensite may be caused by a change in the number of valence electrons per atom as the composition changes [25]. Thus far, observations of the martensitic transformation in bulk CuZr-based shape memory alloys have been of the gradual type [8,26]. The thin-film samples in this study, however, display more complex transformation behavior, from gradual to explosive. Unlike the Fe-Ni system where the explosive transformation is independent of the austenitizing temperature [10], occurrence of the explosive formation of martensite in the CuZr-based systems depends sensitively on the temperature history above A_f . Furthermore, the explosive transformation in CuZrNi results in the complete transformation of the sample instead of just a small fraction as previously observed in other alloy systems. This is clearly the result of an autocatalytic reaction [27], where nucleation of martensite at one site triggers transformation of the entire sample. Given that stress in the austenitic phase promotes the formation of martensite [11,28], it is likely that the stress wave associated with the initial nucleation is sufficient to trigger transformation in neighboring grains, causing the transformation to propagate across the entire sample at nearly the speed of sound. An elastic coupling between transforming grains was observed previously by Machlin and Cohen in Fe-Ni alloys [10]. We believe that a similar process can also form variants within a grain to create a self-accommodating structure with a high density of twins as observed in Fig. 10b.

The observations of explosive transformations in thin-film samples and gradual transformations in bulk samples of CuZr-based alloys are an indication that bulk samples have many more favorable sites that allow simultaneous nucleation of martensite in many grains. In thin-film samples with explosive transformations, by contrast, there are either only a few nucleation sites of weak

potency or nucleation may occur homogenously. For comparison, Olson et al. have reported 10^6 cm⁻³ nucleation sites at $M_{\rm S}$ in the parent phase of ferrous alloys [27]. A similar nucleation site density in CuZr-based alloys would correspond to a single nucleation site in the thin-film samples used in this study. This would suggest a strong size effect in the observed explosive transformation behavior and explain why the behavior is not observed in bulk samples. This size effect has important consequences for the use of this type of shape memory alloys in very small volumes as would be required in micromachined actuators or MEMS.

Samples that have been cycled to a temperature only slightly above A_f transform gradually and nucleation of martensite is not a limiting factor. The TEM images in Fig. 10 indicate that lowtemperature-cycled samples have residual martensite, while hightemperature-cycled samples do not. It is unlikely that the residual martensite is formed during sample preparation because the lift-out process tends to reduce stresses in the sample and makes formation of martensite less likely. Much more likely is the possibility that the sample did not fully transform to austenite on reaching A_f . The residual martensite needs more time to transform back to austenite than provided in the experiments. We suggest that the martensite is stabilized by defects that originate during the martensitic transformation as a result of the large lattice mismatch between the two phases. This scenario is supported by Fig. 7a, which shows that the enthalpy of the reverse transformation peak decreases with additional low-temperature cycles. If a minimum time is required to fully convert the martensite remnants to austenite above A_f, residual martensite should accumulate with additional thermal cycles and the austenitic peak diminish. Once the sample is heated to a more elevated temperature, the defects that stabilize the martensite are annealed, the residual martensite transforms to austenite, and the martensitic transformation reverts to the explosive type.

The kinetics experiments demonstrate that the time required to eliminate the residual martensite is on the order of a few seconds, which makes it difficult to observe this phenomenon in bulk samples. The apparent activation energy of the annihilation process is significantly higher than the activation energy for diffusion. As a reference, the activation energies of both processes are usually similar in steel alloys [29–32]. This results indicates that transformation of the residual martensite to austenite above A_f is a com-

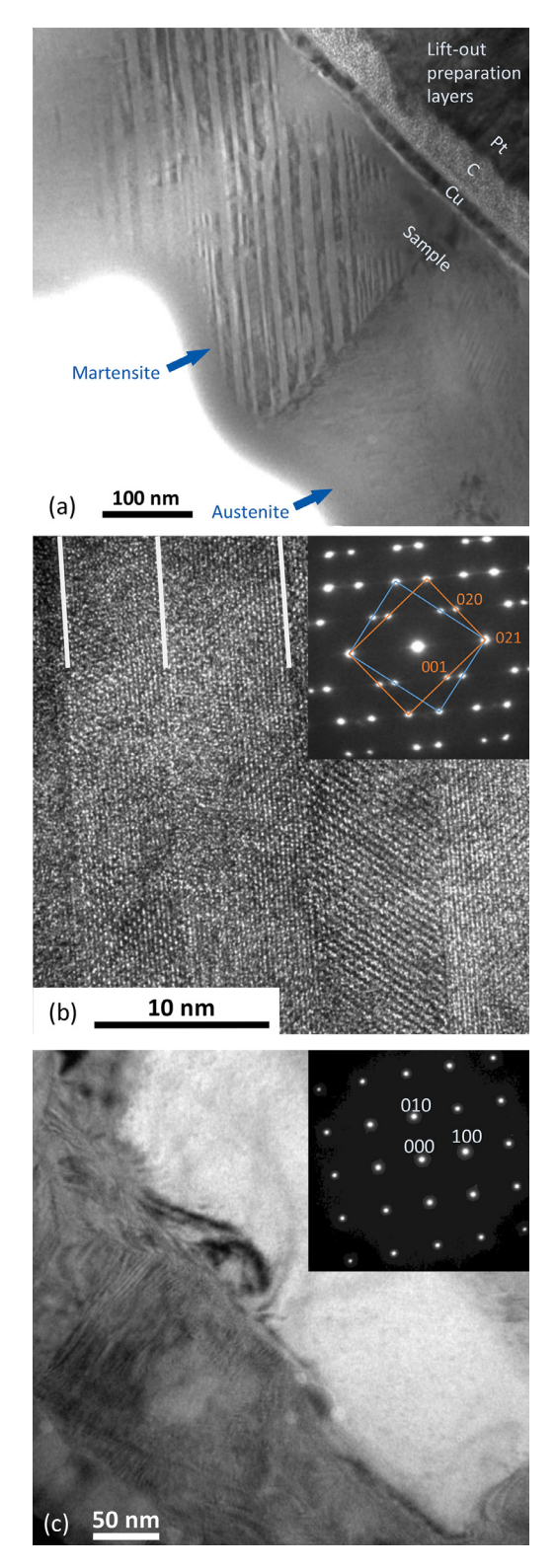


Fig. 10. Transmission electron micrographs of two $Cu_{47}Zr_{49}Co_4$ samples observed at room temperature. (a) The low-temperature cycled sample has a mixture of martensite and austenite. In the top grain, martensite fades into austenite. (b) A high resolution image of martensite twins in (a). The diffraction pattern reveals a (021) twin plane of the Cm space group. (c) The high-temperature cycled sample is fully austenitic. The bottom-left grain shows dense stacking faults, which are visible as dark stripes. The diffraction image is taken on a single grain in the cubic [001] zone axis.

plex process that involves more than just the athermal motion of the interface between the martensite and austenite, or the annihilation by diffusion of defects that stabilize the martensite [33,34].

5. Conclusion

We have investigated the martensitic transformation in thinfilm samples of various CuZr-based shape memory alloys. Nanocalorimetry measurements show that the austenitic phase can be supercooled below M_f , eventually resulting in an explosive transformation to martensite that propagates at a velocity comparable to the speed of sound. The critical transformation temperature depends weakly on cooling rate and changes with composition. Supercooling disappears completely in CuZrNi alloys with Ni content greater than 25 at.%. Whether explosive transformation behavior is observed depends sensitively on the temperature history above the austenite finish temperature A_f . If a sample is quenched immediately after heating above A_f , martensite forms gradually on cooling below M_s ; if a sample is allowed to dwell for a few seconds above A_f , the martensite forms explosively. TEM observations reveal that this behavior is caused by the presence of residual martensite at temperatures above A_f . This martensite is evanescent in the sense that it disappears within a few seconds upon heating above A_f , probably as a result of the annihilation of defects that stabilize the martensite. If this evanescent martensite is retained upon cooling, it facilitates the formation of martensite and the transformation is gradual. If it has disappeared, however, the martensitic transformation is nucleation-limited and becomes explosive.

Declaration of Competing Interest

The authors declare that they have no known competing financial interests or personal relationships that could have appeared to influence the work reported in this paper.

Acknowledgments

This work was supported by the National Science Foundation under Award No. DMR-1808162. It was performed in part at the Center for Nanoscale Systems at Harvard University, which is supported by the National Science Foundation under award No. ECCS-1541959, and at the Materials Research Science and Engineering Center at Harvard University, which is supported by the National Science Foundation under Award No. DMR-2011754. JJV also acknowledges support from the Air Force Office of Scientific Research under Grant No. FA9550-16-10180.

References

- [1] K. Otsuka, X. Ren, Physical metallurgy of Ti-Ni-based shape memory alloys, Prog. Mater. Sci. 50 (2005) 511–678, doi:10.1016/j.pmatsci.2004.10.001.
- [2] J. Ma, I. Karaman, R.D. Noebe, High temperature shape memory alloys, Int. Mater. Rev. 55 (2010) 257–315, doi:10.1179/095066010x12646898728363.
- [3] W.L. Benard, H. Kahn, A.H. Heuer, M.A. Huff, Thin-film shape-memory alloy actuated micropumps, J. Microelectromech. Syst. 7 (1998) 245–251, doi:10.1109/84.679390.
- [4] G.S. Firstov, J. Van Humbeeck, Y.N. Koval, Comparison of high temperature shape memory behaviour for ZrCu-based, Ti-Ni-Zr and Ti-Ni-Hf alloys, Scr. Mater. (2004) 243–248, doi:10.1016/j.scriptamat.2003.09.010.
- [5] G.S. Firstov, J. Van Humbeeck, Y.N. Koval, High temperature shape memory alloys problems and prospects, J. Intell. Mater. Syst. Struct. 17 (2006) 1041–1047, doi:10.1177/1045389X06063922.
- [6] J. Zheng, Y. Miao, H. Zhang, S. Chen, D. Lee, R. Arróyave, J.J. Vlassak, Phase transformations in equiatomic CuZr shape memory thin films analyzed by differential nanocalorimetry, Acta Mater. 159 (2018) 320–331, doi:10.1016/j. actamat.2018.08.015.
- [7] Y. Miao, R. Villarreal, A. Talapatra, R. Arróyave, J.J. Vlassak, Nanocalorimetry and ab initio study of ternary elements in CuZr-based shape memory alloy, Acta Mater. 182 (2020) 29–38, doi:10.1016/j.actamat.2019.10.025.

- [8] G.S. Firstov, J. Van Humbeeck, Y.N. Koval, Peculiarities of the martensitic transformation in ZrCu intermetallic compound potential high temperature SMA, Le J. Phys. IV. 11 (2001) Pr8-481-Pr8-486, doi:10.1051/jp4:2001880.
- [9] D.A. Porter, K.E. Easterling, Phase Transformations in Metals and Alloys, 3rd Ed., CRC Press, 2009, doi:10.1201/9781439883570.
- [10] E.S. Machlin, M. Cohen, Burst phenomenon in the martensitic transformation, J. Met. 3 (1951) 746–754, doi:10.1007/BF03397387.
- [11] R.E. Cech, D. Turnbull, Heterogeneous nucleation of the martensite transformation, JOM 8 (1956) 124–132, doi:10.1007/bf03377656.
- [12] A. Planes, J.L. Macqueron, M. Morin, G. Guénin, L. Delaey, The $\beta \leftrightarrow$ 2H martensitic transformation in a Cu-Zn-Al alloy as studied by simultaneous enthalpy and acoustic emission measurements, Le J. Phys. Colloq. 43 (1982) C4-615-C4-620, doi:10.1051/jphyscol:1982497.
- [13] M.C. Gallardo, J. Manchado, F.J. Romero, J. Del Cerro, E.K.H. Salje, A. Planes, E. Vives, R. Romero, M. Stipcich, Avalanche criticality in the martensitic transition of Cu_{67.64}Zn_{16.71}Al_{15.65} shape-memory alloy: a calorimetric and acoustic emission study, Phys. Rev. B - Condens. Matter Mater. Phys. 81 (2010) 1–8, doi:10.1103/PhysRevB.81.174102.
- [14] P.J. McCluskey, J.J. Vlassak, Combinatorial nanocalorimetry, J. Mater. Res. 25 (2010) 2086–2100, doi:10.1557/jmr.2010.0286.
- [15] K. Xiao, J.M. Gregoire, P.J. McCluskey, J.J. Vlassak, A scanning AC calorimetry technique for the analysis of nano-scale quantities of materials, Rev. Sci. Instrum. 83 (2012), doi:10.1063/1.4763571.
- [16] D. Arias, J.P. Abriata, Cu-Zr (Copper-Zirconium), Bull. Alloy Phase Diagr. 11 (1990) 452–459, doi:10.1007/BF02898260.
- [17] D. Lee, B. Zhao, E. Perim, H. Zhang, P. Gong, Y. Gao, Y. Liu, C. Toher, S. Curtarolo, J. Schroers, J.J. Vlassak, Crystallization behavior upon heating and cooling in Cu₅₀Zr₅₀ metallic glass thin films, Acta Mater. 121 (2016) 68–77, doi:10.1016/J. ACTAMAT.2016.08.076.
- [18] E. Obradó, C. Frontera, L. Mañosa, A. Planes, Order-disorder transitions of Cu-Al-Mn shape-memory alloys, Phys. Rev. B Condens. Matter Mater. Phys. 58 (1998) 14245–14255, doi:10.1103/PhysRevB.58.14245.
- [19] D. Lee, J.J. Vlassak, Diffusion kinetics in binary CuZr and NiZr alloys in the super-cooled liquid and glass states studied by nanocalorimetry, Scr. Mater. 165 (2019) 73–77, doi:10.1016/j.scriptamat.2019.02.014.
- [20] Y. Zhao, T. Pang, J. He, X. Tao, H. Chen, Y. Ouyang, Y. Du, Interdiffusion behaviors and mechanical properties of Cu-Zr system, Calphad Comput. Coupling Phase Diagr. Thermochem. 61 (2018) 92–97, doi:10.1016/j.calphad.2018.02.008.

- [21] D. Schryvers, G.S. Firstov, J.W. Seo, J. Van Humbeeck, Y.N. Koval, Unit cell determination in CuZr martensite by electron microscopy and X-ray diffraction, Scr. Mater. 36 (1997) 1119–1125, doi:10.1016/S1359-6462(97)00003-1.
- [22] J.W. Seo, D. Schryvers, TEM investigation of the microstructure and defects of CuZr martensite. Part I: morphology and twin systems, Acta Mater. 46 (1998) 1165–1175, doi:10.1016/S1359-6454(97)00333-9.
- [23] M. Ueda, H.Y. Yasuda, Y. Umakoshi, Effect of grain boundary character on the martensitic transformation in Fe-32at. Ni bicrystals, Acta Mater. 49 (2001) 3421–3432, doi:10.1016/S1359-6454(01)00252-X.
- [24] M. Cohen, Martensitic nucleation revisited, Mater. Trans. JIM 33 (1992) 178– 183, doi:10.2320/matertrans1989.33.178.
- [25] E. Obradó, L. Mañosa, A. Planes, Stability of the bcc phase of Cu-Al-Mn shape-memory alloys, Phys. Rev. B Condens. Matter Mater. Phys. 56 (1997) 20–23, doi:10.1103/PhysRevB.56.20.
- [26] F. Meng, K. Tsuchiya, S. Ii, Y. Yokoyama, Influence of Ni on stability of martensitic transformation in Zr₅₀Cu_{50-x}Ni_x, J. Alloys Compd. 577 (2013) 136–140, doi:10.1016/j.jallcom.2012.01.089.
- [27] G.B. Olson, M. Cohen, A perspective on martensitic nucleation, Annu. Rev. Mater. Sci. 11 (1981) 1–32, doi:10.1146/annurev.ms.11.080181.000245.
- [28] S.A. Kulin, M. Cohen, B.L. Averbach, Effect of applied stress on the martensitic transformation, JOM 4 (1952) 661–668, doi:10.1007/bf03397742.
- [29] R. Schnitzer, R. Radis, M. Nöhrer, M. Schober, R. Hochfellner, S. Zinner, E. Povoden-Karadeniz, E. Kozeschnik, H. Leitner, Reverted austenite in PH 13-8 Mo maraging steels, Mater. Chem. Phys. 122 (2010) 138–145, doi:10.1016/j.matchemphys.2010.02.058.
- [30] G.P. Krielaart, S. Van Der Zwaag, Kinetics of $\gamma \rightarrow \gamma$ phase transformation in Fe-Mn alloys containing low manganese, Mater. Sci. Technol. 14 (1998) 10–18, doi:10.1179/mst.1998.14.1.10.
- [31] R.G. Thiessen, I.M. Richardson, J. Sietsma, Physically based modelling of phase transformations during welding of low-carbon steel, Mater. Sci. Eng. A 427 (2006) 223–231, doi:10.1016/j.msea.2006.04.076.
- [32] A. Bojack, L. Zhao, P.F. Morris, J. Sietsma, Austenite formation from martensite in a 13Cr6Ni2Mo supermartensitic stainless steel, Metall. Mater. Trans. A. 47 (2016), doi:10.1007/s11661-016-3404-z.
- [33] M. Grujicic, G.B. Olson, W.S. Owen, Mobility of martensitic interfaces, Metall. Trans. A 16 (1985) 1713–1722, doi:10.1007/BF02670359.
- [34] M. Grujicic, G.B. Olson, W.S. Owen, Mobility of the β 1- γ 1' martensitic interface in Cu-Al-Ni: Part I. Experimental measurements, Metall. Trans. A 16 (1985) 1723–1734, doi:10.1007/BF02670360.